3

Statistical Properties of Surface Slopes via Remote Sensing

Josué Álvarez-Borrego[1] and Beatriz Martín-Atienza[2]
[1]*CICESE, División de Física Aplicada, Departamento de Óptica*
[2]*Facultad de Ciencias Marinas, UABC*
México

1. Introduction

The complexity of wave motion in deep waters, which can damage marine platforms and vessels, and in shallow waters, same that can afflict human settlements and recreational areas, has given origin to a long-term development in laboratory and field studies, the conclusions of which are used to design methodology and set bases to understand wave motion behavior.

Via remote sensing, the use of radar images and optical processing of aerial photographs has been used. The interest in wave data is manifold; one element is the inherent interest in the directional spectra of waves and how they influence the marine environment and the coastline. These wave data can be readily and accurately collected by aerial photographs of the wave sun glint patterns which show reflections of the Sun and sky light from the water and thus offer high-contrast wave images.

In a series of articles, Cox and Munk (1954a, 1954b, 1955) studied the distribution of intensity or glitter pattern in aerial photographs of the sea. One of their conclusions was that for constant and moderate wind speed, the probability density function of the slopes is approximately Gaussian. This could be taken as an indication that in certain circumstances, the ocean surface could be modeled as a Gaussian random process. Similar observations by Longuet-Higgins et al. (1963) (cited by Longuet-Higgins (1962)) with a floating buoy, which filters out the high-frequency components, come considerably closer to the Gaussian distribution.

Other authors (Stilwell, 1969; Stilwell & Pilon, 1974) have studied the same problem considering a sea surface illuminated by a continuous sky light with no azimuthal variations in sky radiance. Different models of sky light have been used emphasizing the existence of a nonlinear relationship between the slope spectrum and the corresponding wave image spectrum (Peppers & Ostrem, 1978; Chapman & Irani, 1981).

Simulated sea surfaces have been analyzed by optical systems to understand the optical technique in order to obtain best qualitative information of the spectrum (Álvarez-Borrego, 1987; Álvarez-Borrego & Machado, 1985).

Fuks and Charnotskii (2006) derived the joint probability density function of surface height and partial second derivatives for an ensemble of specular points at a random rough Gaussian isotropic surface at normal incidence. However, in a real physical situation, consideration of Gaussian statistics can be a very good approximation.

Cox and Munk (1956) observed that the center of the glitter pattern images had shifted downwind from the grid center. This shift can be associated with an up/downwind asymmetry of the wave profile (Munk, 2009). Surfaces of small positive slope are more probable than those of negative slope; large positive slopes are less probable than larger negative slopes, thus permitting the restraint of a zero mean slope (Bréon & Henrist, 2006).

According with Longuet-Higgins (1963) the sea surface slopes have a Gaussian probability function to a first approximation. In the next approximation skewness is taken into account. The kurtosis is zero, as are all the higher cumulants. In the next approximation, the distribution is given taken into account the kurtosis.

Walter Munk (2009) writes that the skewness appears to be correlated with a rather sudden onset of breaking for winds above 4 m s^{-1} and he does not think that skewness comes from parasitic capillaries. Chapron et al. (2002) suggest that the actual waves form under near-breaking conditions, along with the varying population and length scales for these breaking events, should also contribute to the skewness.

In this chapter we will consider two different cases to analyze statistical properties of surface slopes via remote sensing: first we assume the fluctuation of the surface slopes to be statistically Gaussian and the second case we assume the fluctuation of the surface slopes to be statistically non-Gaussian. We, also, assume that the surfaces are illuminated by a source, the Sun, of a fixed angular extent, β, and imaged through a lens that subtends a very small solid angle. With these considerations, we calculated their images, as they would be formed by a signal clipping detector. In order to do this, we define a "glitter function", which operates on the slope of the surfaces. In the first case we consider two situations: the detector line of sight angle, θ_d, is constant for each point on the surface and θ_d is variable for each point in the surface. In the second case, with non-Gaussian statistics, we consider θ_d variable for each point in the surface only, because we consider that this case is more realistic.

2. Geometry of the model (Gaussian case considering a constant detector angle)

The physical situation is shown in figure 1. The surface $\zeta(x)$ is illuminated by a uniform incoherent source S of limited angular extent, with wavelength $\bar{\lambda}$. Its image is formed in D by an aberration free optical system. The incidence angle, θ_s, is defined as the angle between the incidence angle direction and the normal to the mean surface. Then, in figure 1, θ_s, represents the mean angle subtended by the source S and θ_d represents the mean angle subtended by the optical system of the detector with the normal to the mean surface.

The apparent diameter of the source is β and of the detector is δd. Light from the source is reflected on the surface just one time and, depending on the slope, the light reflected will or will not be part of the image. In broad terms, the image consists of bright and dark regions that we call a glitter pattern. α represents the angle between the x axis and the surface, and

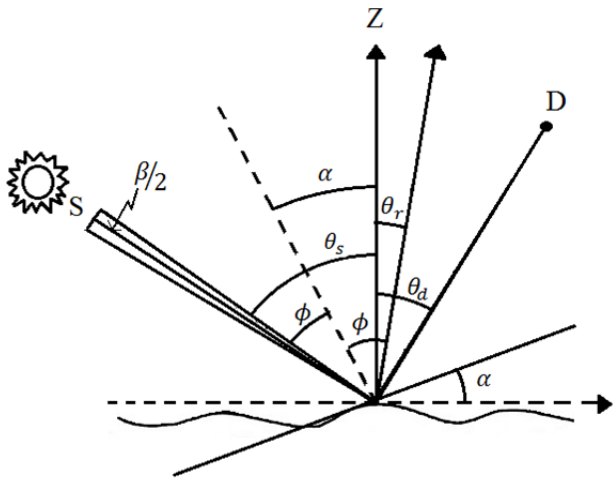

Fig. 1. The detector is located in the zenith of each reflection point in the profile.

ϕ represents the angle between the normal to the plane and the source S. This angle is given by $\phi = \theta_s - \alpha$, and the specular angle is given by $\phi = \theta_r + \alpha$. From this two equations we can write

$$\theta_r = \theta_s - 2\alpha \ . \tag{1}$$

Because the source has a finite size, there are several incidence directions which are specular reflected to the camera. The directions, θ_{os} (where this angle is the angular dimension of the Sun), where there are incidence rays which are determined by the condition

$$\theta_s - \frac{\beta}{2} \le \theta_{os} \le \theta_s + \frac{\beta}{2}, \tag{2}$$

in other words, the source is angularly described by the function, $\sigma(\theta_{os})$, can be written like

$$\sigma(\theta_{os}) = rect\left[\frac{\theta_{os} - \theta_s}{\beta}\right], \tag{3}$$

where rect(.) represents the rectangle function (Gaskill, 1978).

So, the projection of this source on the detector, after reflection, is given by

$$\theta_s - \frac{\beta}{2} - 2\alpha \le \theta \le \theta_s + \frac{\beta}{2} - 2\alpha \ , \tag{4}$$

$$\sigma_R(\theta) = rect\left(\frac{\theta - \theta_r}{\beta}\right), \tag{5}$$

where equation (1) is taken into account.

On the other side, the detection system pupil can be represented by the function

$$P(\theta) = rect\left(\frac{\theta - \theta_d}{\delta d}\right). \tag{6}$$

The intensity light I, arriving to the detection plane D depends on the overlap between the functions $\sigma_R(\theta)$ and $P(\theta)$, and can be approximated by

$$I = \int_{-\frac{\pi}{2}}^{\frac{\pi}{2}} \sigma_R(\theta) P(\theta) d\theta. \tag{7}$$

In practical situations δd is so smaller than β, that we can to approximate $P(\theta) = \delta(\theta - \theta_d)$, where δ is the Dirac delta, of this way

$$\begin{aligned} I &\approx \sigma_R(\theta_d), \\ &\approx rect\left(\frac{\theta_d - \theta_r}{\beta}\right). \end{aligned} \tag{8}$$

The light reflection will arrive to the detector D when

$$\theta_r - \frac{\beta}{2} \le \theta_d \le \theta_r + \frac{\beta}{2}, \tag{9}$$

and because $\theta_r = \theta_s - 2\alpha$, we have

$$\frac{\theta_s - \theta_d}{2} - \frac{\beta}{4} \le \alpha \le \frac{\theta_s - \theta_d}{2} + \frac{\beta}{4}. \tag{10}$$

Defining $\Pi = \tan\alpha$, $\gamma = (\theta_s - \theta_d)/2$ and $\Pi_o = \tan\gamma$, and using the relationship $\tan(\gamma \pm \beta/4) \approx \tan\gamma \pm \left(1 + \tan^2\gamma\right)\beta/4$, valid for small $\beta/4$, we obtain the next condition for the slopes

$$\Pi_o - \left(1 + \Pi_o^2\right)\frac{\beta}{4} \le \Pi \le \Pi_o + \left(1 + \Pi_o^2\right)\frac{\beta}{4}. \tag{11}$$

We find then the "glitter function", given by

$$B(\Pi) = rect\left[\frac{\Pi - \Pi_o}{\left(1 + \Pi_o^2\right)\beta/2}\right]. \tag{12}$$

This expression (eq. 12) tell us that the geometry of the problem selects a surface slope region and encodes like bright points in the image (glitter pattern).

2.1 Relationship among the variances of the intensities in the image, surface slopes and surface heights

The mean of the image, μ_I, may be written (Papoulis, 1981)

$$\mu_I = \langle I(x) \rangle = \int_{-\infty}^{+\infty} B(\Pi) p(\Pi) d\Pi, \tag{13}$$

where $B(\Pi)$ is defined by equation (12) and $p(\Pi)$ is the probability density function in one dimension, where in a first approximation a Gaussian function is considered. Substituting in equation (13) the expressions for $B(\Pi)$ and $p(\Pi)$, we have

$$\mu_I = \langle I(x) \rangle = \frac{1}{\sigma_\Pi (2\pi)^{1/2}} \int_{-\infty}^{\infty} rect\left[\frac{\Pi - \Pi_o}{\left(1+\Pi_o^2\right)\beta/2} \right] \exp\left(-\frac{\Pi^2}{2\sigma_\Pi^2} \right) d\Pi. \tag{14}$$

Defining $a = \Pi_o - \left(1+\Pi_o^2\right)(\beta/4)$ and $b = \Pi_o + \left(1+\Pi_o^2\right)(\beta/4)$, we can write

$$\mu_I = \langle I(x) \rangle = \frac{1}{2}\left[erf\left(\frac{b}{\sqrt{2}\sigma_\Pi} \right) - erf\left(\frac{a}{\sqrt{2}\sigma_\Pi} \right) \right]. \tag{15}$$

The variance of the intensities in the image, σ_I^2, is defined by (Papoulis, 1981)

$$\sigma_I^2 = \langle I^2(x) \rangle - \langle I(x) \rangle^2 = \int_{-\infty}^{+\infty} \left[B(\Pi) - \mu_I \right]^2 p(\Pi) d\Pi. \tag{16}$$

But, $B(\Pi) = B^2(\Pi)$, then $\langle I^2(x) \rangle = \langle I(x) \rangle$, therefore

$$\sigma_I^2 = \langle I(x) \rangle - \langle I(x) \rangle^2 = \mu_I (1 - \mu_I), \tag{17}$$

and substituting the expression of $\langle I(x) \rangle$, equation (15), in equation (17), we have

$$\sigma_I^2 = \frac{1}{2}\left[erf\left(\frac{b}{\sqrt{2}\sigma_\Pi} \right) - erf\left(\frac{a}{\sqrt{2}\sigma_\Pi} \right) \right] - \left(\frac{1}{2}\left[erf\left(\frac{b}{\sqrt{2}\sigma_\Pi} \right) - erf\left(\frac{a}{\sqrt{2}\sigma_\Pi} \right) \right] \right)^2, \tag{18}$$

which is the required relation between the variance of the intensities in the image, σ_I^2, and the variance of the surface slopes, σ_Π^2.

The relation (18) is shown in figure 2 for some typical cases, using the geometry described above, with $\theta_d = 0^o$ and $\beta = 0.68^o$. In the horizontal axis we have the variance of the surface slopes, σ_Π^2, and in the vertical axis we have the variance of the intensities of the image, σ_I^2. In the figure we can observe the dependence of this relationship with the angular position of the source, θ_s. In figure 2 we also can observe that for small incidence angles (0-10 degrees) and small values of variance of the surface slopes, it is possible to obtain bigger values in the variance of the intensities in the image. From equation (18), we can see that this behavior is

independent of any surface height power spectrum that we are analyzing, because this relation depends on the probability density function of the surface slopes and the geometry of the experiment only.

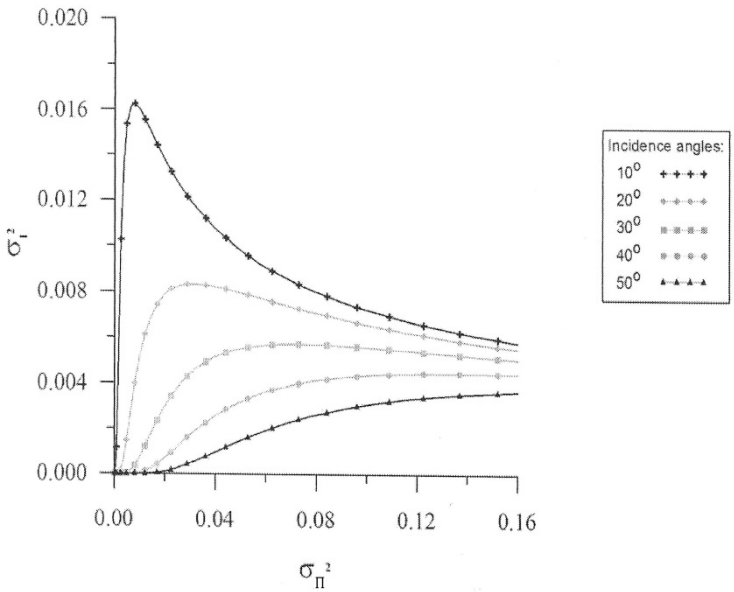

Fig. 2. Relationship between the variance of the surface slopes with the variance of the intensities in the image.

In certain cases, figure 2, if we have data corresponding to a θ_s value only, it is not possible to obtain the variance of the surface slopes, σ_Π^2, because for a value of σ_I^2 we will have two possible values of σ_Π^2. To solve this problem, it is necessary to analyze images which correspond at two or more incidence angles and to select a slope variance value which is consistent with all these data.

The relationship between σ_Π^2 and σ_ζ^2 can be derived from (Papoulis, 1981)

$$C_\Pi(\tau) = -\frac{d^2 C_\zeta(\tau)}{d\tau^2}, \tag{19}$$

if we know the correlation function of the surface heights (this will be shown in next section of this chapter). Here, $C_\zeta(\tau)$ is the correlation function of the surface heights and $C_\Pi(\tau)$ is the correlation function of the surface slopes.

2.2 Relationship between the correlation function of the intensities in the image and of the surface heights

Our analysis involves three random processes: the surface profile, $\zeta(x)$, its surface slopes, $\Pi(x)$, and the image, $I(x)$. Each process has a correlation function and it was shown (Álvarez-Borrego, 1993) that these three functions hold a relationship.

The relationship between correlation functions of the surface heights, $C_\zeta(\tau)$, and the surface slopes, $C_\Pi(\tau)$, is given by equation (19), and the relationship between $C_\Pi(\tau)$ and the correlation function of the intensities in the image, $C_I(\tau)$, is given by (Álvarez-Borrego, 1993)

$$\sigma_I^2 C_I(\tau) = \int_{-\infty}^{\infty}\int_{-\infty}^{\infty} \frac{B(\Pi_1)B(\Pi_2)}{2\pi\sigma_\Pi^2\left[1-C_\Pi^2(\tau)\right]^{1/2}} \exp\left[-\frac{\Pi_1^2+\Pi_2^2-2C_\Pi(\tau)\Pi_1\Pi_2}{2\sigma_\Pi^2\left[1-C_\Pi^2(\tau)\right]}\right] d\Pi_1 d\Pi_2 . \quad (20)$$

In order to achieve the inverse process, using equation (19) and equation (20), these two equations must meet certain conditions. For example, it is required that there exists one to one correspondence among the amount involved.

Using equation (19) the processed data can be numerically integrated twice, such that we obtain information of the correlation function of the surface heights, $C_\zeta(\tau)$, from the correlation function of the surface slopes, $C_\Pi(\tau)$. Although equation (20) is a more complicated expression, we cannot obtain an analytical result from it. A first integral can be analytically solved and for the second it is possible to obtain the solution by numerical integration. Resolving the first integral analytically, equation (20) can be written like

$$\sigma_I^2 C_I(\tau) = \int_a^b \frac{\sqrt{2}}{4\sigma_\Pi\sqrt{\pi}} \exp\left[-\frac{\Pi_2^2}{2\sigma_\Pi^2}\right]\left\{erf\left(\frac{b-C_\Pi(\tau)\Pi_2}{\sqrt{2\sigma_\Pi^2\left[1-C_\Pi^2(\tau)\right]}}\right) - erf\left(\frac{a-C_\Pi(\tau)\Pi_2}{\sqrt{2\sigma_\Pi^2\left[1-C_\Pi^2(\tau)\right]}}\right)\right\} d\Pi_2 , \quad (21)$$

where $a = \Pi_o - \left(1+\Pi_o^2\right)\beta/4$ and $b = \Pi_o + \left(1+\Pi_o^2\right)\beta/4$.

So, a relationship between values of the correlation function of the intensities in the image, $C_I(\tau)$, and the values of the correlation function of the surface slopes takes, $C_\Pi(\tau)$, can be obtained (Figure 3). In this case, to small angles we can find higher values for the correlation function of the intensities in the image. In all the cases, the angular position of the camera or detector, θ_d, is zero and σ_Π^2 =0.03 . The correlation functions of figure 3 are normalized.

Also, from equation (19), it is possible to obtain the correlation function of the surface heights, $C_\zeta(\tau)$, from $C_\Pi(\tau)$ and the require inverse process to determine the correlation function of the surface heights is completed.

A theoretical variance σ_I^2 can be calculated from equation (21). We wrote in Table 1 the values of the image variance in order to normalize the correlations in figure 3 for different values for θ_s.

θ_s	σ_Π^2	σ_I^2
10	0.03	0.0119734700
20	0.03	0.0083223130
30	0.03	0.0044081650
40	0.03	0.0016988780
50	0.03	0.0004438386

Table 1. Values of the image variance in order to normalize the correlations in figure 3 for different values for θ_s.

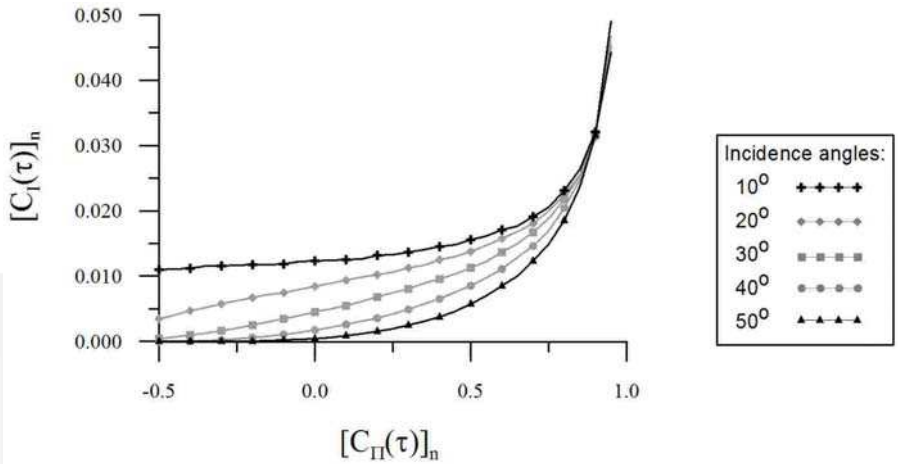

Fig. 3. Relationship between the correlation function of the surface slopes and the correlation function of the intensities in the image.

3. Geometry of the model (Gaussian case considering a variable detector angle)

A more real physical situation is shown in figure 4. The surface, $\zeta(x)$, is illuminated by a uniform incoherent source S of limited angular extent, with wavelength $\bar{\lambda}$. Its image is formed in D by an aberration-free optical system. The incidence angle θ_s is defined as the angle between the incidence angle direction and the normal to the mean surface and represents the mean angle subtended by the source S. $(\theta_d)_i$ corresponds to the angle subtended by the optical system of the detector with the normal to point i of the surface, i. e.

$$(\theta_d)_i = \tan^{-1}\left(\frac{i\Delta x}{H}\right), \tag{22}$$

where H is the height of the detector and Δx is the interval between surface points. We can see that in this more realistic physical situation, angle θ_d is changing with respect to each point in the surface. It is worth noticing that a variable θ_d does not restrict the sensor field of view.

α_i is the angle subtended between the normal to the mean surface and the normal to the slope for each i point in the surface

$$\alpha_i = \frac{\theta_s + (\theta_d)_i}{2} = \frac{\theta_s}{2} + \frac{1}{2}\tan^{-1}\left(\frac{i\Delta x}{H}\right). \tag{23}$$

The apparent diameter of the source is β. Light from the source is reflected on the surface for just one time, and, depending on the slope, the light reflected will or will not be part of the image. Thus, the image consists of bright and dark regions that we call a glitter pattern.

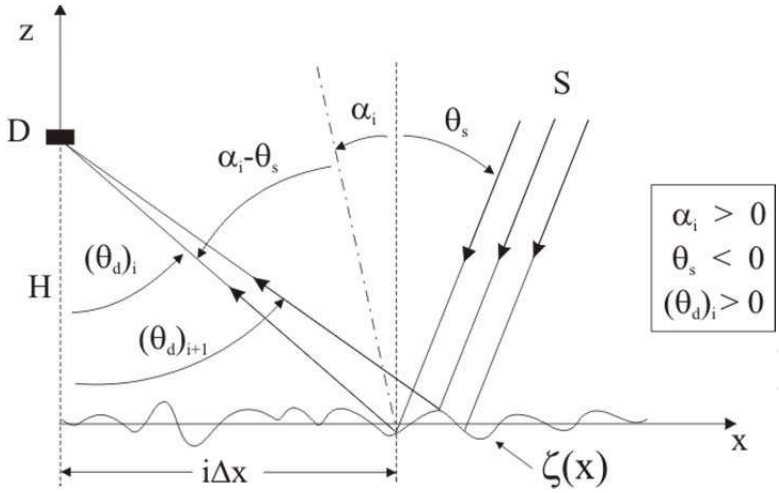

Fig. 4. Geometry of the real physical situation. Counterclockwise angles are considered as positive and clockwise angles as negative.

The glitter function can be expressed as (Álvarez-Borrego & Martín-Atienza, 2010)

$$B(\Pi_i) = rect\left[\frac{\Pi_i - \Pi_{oi}}{\left(1+\Pi_{oi}^2\right)\frac{\beta}{2}}\right], \tag{24}$$

where

$$\Pi_{oi} - \left(1+\Pi_{oi}^2\right)\frac{\beta}{4} \le \Pi_i \le \Pi_{oi} + \left(1+\Pi_{oi}^2\right)\frac{\beta}{4}, \tag{25}$$

$$\Pi_i = \tan(\alpha_i), \tag{26}$$

$$\Pi_{oi} = \tan\left[\frac{\theta_s + (\theta_d)_i}{2}\right]. \tag{27}$$

The interval characterized by equation (25) defines a specular band where certain slopes generate bright spots in the image. This band has now a nonlinear slope due to the variation of $(\theta_d)_i$ with respect to each i point of the surface (Figure 5). Combining equations (25) – (27), the slope interval, where a bright spot is received by the detector, is

$$\frac{\theta_s}{2} + \frac{1}{2}\tan^{-1}\left(\frac{i\Delta x}{H}\right) - \frac{\beta}{4} \le \alpha_i \le \frac{\theta_s}{2} + \frac{1}{2}\tan^{-1}\left(\frac{i\Delta x}{H}\right) + \frac{\beta}{4}. \tag{28}$$

3.1 Relationships among the variances of the intensities in the image and surface slopes

The mean of the image μ_I may be written as (Álvarez-Borrego & Martín-Atienza, 2010)

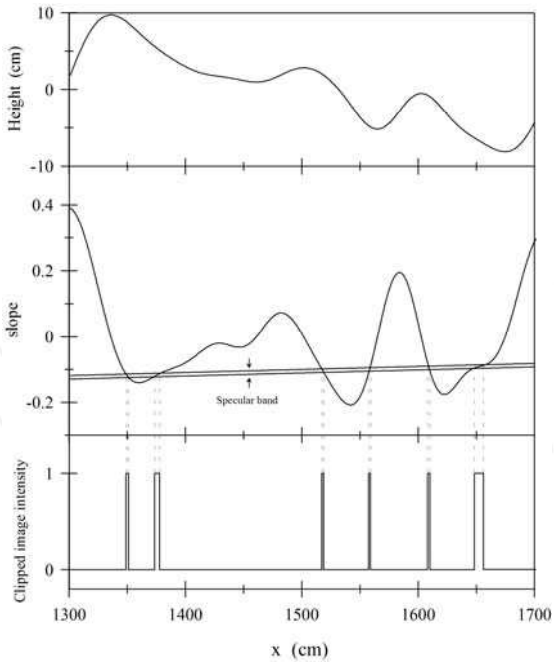

Fig. 5. All the random processes involved in our analysis. The specular band corresponds to bright regions in the image.

$$\mu_I = \langle I(x) \rangle = \int_{-\infty}^{\infty} B(\Pi_i) p(\Pi_i) d\Pi_i, \tag{29}$$

where $B(\Pi_i)$ is the glitter function defined be equation (24). $p(\Pi_i)$ is the probability density function, where a Gaussian function is considered in one dimension. Substituting in equation (29) the expressions for $B(\Pi_i)$ and $p(\Pi_i)$, we have

$$\mu_I = \langle I(x) \rangle = \frac{1}{N} \sum_{i=1}^{N} \frac{1}{\sigma_\Pi \sqrt{2\pi}} \int_{-\infty}^{\infty} rect\left[\frac{\Pi_i - \Pi_{oi}}{\left(1 + \Pi_{oi}^2\right) \frac{\beta}{2}} \right] \exp\left(-\frac{\Pi_i^2}{2\sigma_\Pi^2} \right) d\Pi_i. \tag{30}$$

The detector angle θ_d is a function of the position x; thus, the specular angle is a function of the distance x from the nadir point of the detector $n = 0$ to the point $n = i$ (equation 22).

Defining $a_i = \Pi_{oi} - \left(1 + \Pi_{oi}^2\right)\beta/4$ and $b_i = \Pi_{oi} + \left(1 + \Pi_{oi}^2\right)\beta/4$, we can write

$$\mu_I = \langle I(x) \rangle = \frac{1}{N} \sum_{i=1}^{N} \frac{1}{2} \left[erf\left(\frac{b_i}{\sqrt{2}\sigma_\Pi} \right) - erf\left(\frac{a_i}{\sqrt{2}\sigma_\Pi} \right) \right]. \tag{31}$$

The variance of the intensities in the image σ_I^2 is defined by (Álvarez-Borrego & Martín-Atienza, 2010)

$$\sigma_I^2 = \left\langle I^2(x) \right\rangle - \left\langle I(x) \right\rangle^2 = \frac{1}{N}\sum_{i=1}^{N}\int_{-\infty}^{+\infty}\left[B(\Pi_i) - \mu_I\right]^2 p(\Pi_i)\, d\Pi_i. \tag{32}$$

However, $B(\Pi_i) = B^2(\Pi_i)$, then $\left\langle I^2(x) \right\rangle = \left\langle I(x) \right\rangle$; therefore

$$\sigma_I^2 = \left\langle I(x) \right\rangle - \left\langle I(x) \right\rangle^2 = \mu_I(1 - \mu_I). \tag{33}$$

Substituting the equation (31) in equation (33), we have

$$\sigma_I^2 = \frac{1}{N}\sum_{i=1}^{N}\left\{\frac{1}{2}\left[erf\left(\frac{b_i}{\sqrt{2}\sigma_\Pi}\right) - erf\left(\frac{a_i}{\sqrt{2}\sigma_\Pi}\right)\right] - \frac{1}{4N}\left[erf\left(\frac{b_i}{\sqrt{2}\sigma_\Pi}\right) - erf\left(\frac{a_i}{\sqrt{2}\sigma_\Pi}\right)\right]^2\right\}, \tag{34}$$

which is the required relationship between the variance of the intensities in the image σ_I^2 and the variance of the surface slopes σ_Π^2.

The relationship between the variance of the surface slopes and the variances of the intensities of the image for different θ_s angles (10º-50º) is shown in figure 6 (equation 34). The detector is located as shown in figure 4 and the subtended angle by the source is $\beta = 0.68^o$. When the camera detector is at H=100 m the behavior of the curves look similar to the curves shown in Álvarez-Borrego & Martín-Atienza, 2010 (figure 6a). In this case, we also can observe that, for big incidence angles (40º – 50º) and small values of variance of the surface slopes, it is possible to obtain bigger values in the variance of the intensities in the image.

If we analyze the figure 6j we can observe that σ_I^2 increases for lower θ_s values (10º-20º). These results match with the results presented by Álvarez-Borrego in 1993. Figure 6j was made considering an H=1000 m. The reason for this match is that the condition proposed by Álvarez-Borrego in 1993 considers a θ_d value constant (see figure 2). This condition is similar to have the sensor camera to an H value very high where the surface slopes values are considered almost constant.

Figure 6 shows how these relationships (σ_I^2 versus σ_Π^2) are changing while H is being bigger. Dark lines show limit extremes for θ_s of 10º and 50º. It can be seen that when H is increasing to 200 m the line of 50º starts to decay and start to cross with the others. In so far as H goes up, the lines, with larger θ_s go down until the order of the curves change. The explanation for this is very simple: if the camera stays at H=100 m, it will receive more reflection of light at large θ_s, because the geometry of reflection. When H increases, the camera will receive less light reflection of large incidence angles but will have more light reflection for small incidence angles. Therefore, when the camera is at a larger height, will have more reflection from light incidence angles smaller than light of larger incidence angles. Thus we can say that the results presented by Álvarez-Borrego in 1993, Cureton *et al.*, 2007 and Álvarez-Borrego & Martín-Atienza in 2010 are correct for the Gaussian case.

In certain cases, if we have data corresponding to one θ_s value, it is not possible to obtain a single value for the variance of the surface slopes σ_Π^2. To solve this problem, it is necessary to analyze images which correspond at two or more incidence angles and to select a slope variance value which is consistent with all these data (Álvarez-Borrego, 1995).

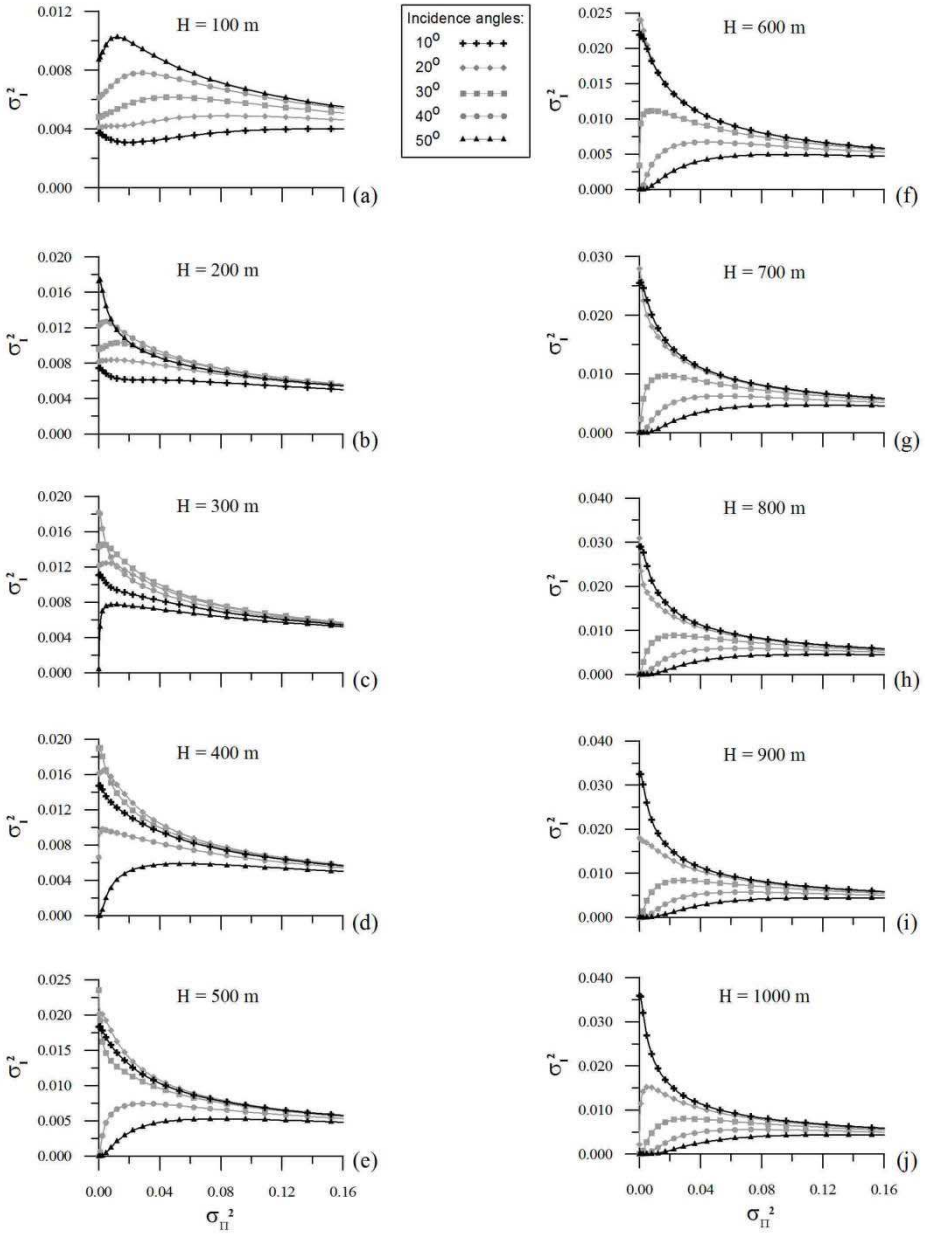

Fig. 6. Relationship between the variance of the surface slopes and the variance of the intensities of the image for different H values.

From equation (34), we can see that this relation depends on the probability density function of the surface slopes and the geometry of the experiment only.

3.2 Relationship between the correlation functions of the intensities in the image and of the surface slope

The relationship between the correlation function of the surface slopes $C_\Pi(\tau)$ and the correlation functions of the intensities in the image $C_I(\tau)$ is given by

$$\sigma_I^2 C_I(\tau) = \frac{1}{N}\sum_{i=1}^{N}\int_{-\infty}^{\infty}\frac{1}{N}\sum_{i=1}^{N}\int_{-\infty}^{\infty} B(\Pi_{1i})B(\Pi_{2i})p(\Pi_{1i},\Pi_{2i})d\Pi_{1i}\,d\Pi_{2i}, \tag{35}$$

where $p(\Pi_{1i},\Pi_{2i})$ is defined by

$$p(\Pi_{1i},\Pi_{2i}) = \frac{1}{2\pi\sigma_\Pi^2\left[1-C_\Pi^2(\tau)\right]^{1/2}}\exp\left[-\frac{\Pi_{1i}^2 - 2C_\Pi(\tau)\Pi_{1i}\Pi_{2i} + \Pi_{2i}^2}{2\sigma_\Pi^2\left(1-C_\Pi^2(\tau)\right)}\right]. \tag{36}$$

Although it is possible to obtain an analytical relationship for the first integral, for the second integral the process must be numeric. Thus, eq. (35) can be written like

$$\sigma_I^2 C_I(\tau) = \frac{1}{N}\sum_{i=1}^{N}\int_{a_i}^{b_i}\frac{1}{N}\sum_{i=1}^{N}\frac{\sqrt{2}}{4\sigma_\Pi\sqrt{\pi}}\exp\left[-\frac{\Pi_2^2}{2\sigma_\Pi^2}\right]\left\{erf\left(\frac{b_i - C_\Pi(\tau)\Pi_2}{\sqrt{2\sigma_\Pi^2\left[1-C_\Pi^2(\tau)\right]}}\right) - erf\left(\frac{a_i - C_\Pi(\tau)\Pi_2}{\sqrt{2\sigma_\Pi^2\left[1-C_\Pi^2(\tau)\right]}}\right)\right\}d\Pi_2, \tag{37}$$

where $a_i = \Pi_{oi} - \left(1+\Pi_{oi}^2\right)\beta/4$ and $b_i = \Pi_{oi} + \left(1+\Pi_{oi}^2\right)\beta/4$.

In order to avoid computer memory problems, the 16384 data point profile was divided into into a number of consecutive intervals. The value of θ_d varies point to point in the profile. For each interval and for each θ_s value, the relationship between the correlation functions $C_I(\tau)$ and $C_\Pi(\tau)$ was calculated. Then, the several computed relationships for each θ_s value were averaged.

In this case we used a value of σ_Π^2 =0.03 . The correlation function of the intensities in the image is not normalized. Similar to the behavior of the variances, when H increases the behavior of the curves have a similar process. A theoretical variance σ_I^2 can be calculated from equation (37). We wrote in Table 2 the values of the image variance in order to normalize the correlations in figure 7 for different values for θ_s and H (100, 500, 1000 and 5000 m).

4. Geometry of the model (Non-Gaussian case considering a variable detector angle)

The model, considering θ_d as variable, is shown in figure 4. We think this is a more realistic situation.

4.1 Relationships among the variances of the intensities in the image and surface slopes considering a non-Gaussian probability density function

The mean of the image μ_I may be written as (Álvarez-Borrego & Martín-Atienza, 2010):

H	θ_s	σ_Π^2	σ_I^2
100	10	0.03	0.00003160564
100	20	0.03	0.00005271762
100	30	0.03	0.00014855790
100	40	0.03	0.00058990210
100	50	0.03	0.00195377600
500	10	0.03	0.00015853820
500	20	0.03	0.00023902050
500	30	0.03	0.00043911520
500	40	0.03	0.00107317300
500	50	0.03	0.00269619900
1000	10	0.03	0.00031712280
1000	20	0.03	0.00047002010
1000	30	0.03	0.00078709770
1000	40	0.03	0.00161060600
1000	50	0.03	0.00344703200
5000	10	0.03	0.00158160000
5000	20	0.03	0.00228022000
5000	30	0.03	0.00332568200
5000	40	0.03	0.00498063700
5000	50	0.03	0.00723998800

Table 2. Values of the image variance in order to normalize the correlations in figure 7 for different values for θ_s and H.

$$\mu_I = \langle I(x) \rangle = \frac{1}{N} \sum_{i=1}^{N} \int_{-\infty}^{+\infty} B(\Pi_i) p(\Pi_i) d\Pi_i \tag{38}$$

where $B(\Pi_i)$ is the glitter function defined by equation (24). $p(\Pi_i)$ is the probability density function, where a non-Gaussian function is considered in one dimension (Cureton, 2010)

$$p(\Pi_i) = \frac{1}{\sigma_\Pi \sqrt{2\pi}} \exp\left(-\frac{\Pi_i^2}{2\sigma_\Pi^2} \right) \bullet \left[1 + \frac{1}{6} \lambda_\Pi^{(3)} \left\{ \left(\frac{\Pi_i}{\sigma_\Pi} \right)^3 - 3 \left(\frac{\Pi_i}{\sigma_\Pi} \right) \right\} + \frac{1}{24} \lambda_\Pi^{(4)} \left\{ \left(\frac{\Pi_i}{\sigma_\Pi} \right)^4 - 6 \left(\frac{\Pi_i}{\sigma_\Pi} \right)^2 + 3 \right\} \right], \tag{39}$$

where $\lambda_\Pi^{(3)}$ is the skewness, $\lambda_\Pi^{(4)}$ is the kurtosis and σ_Π is the standard deviation of the surface slopes.

Substituting in equation (38) the expressions for $B(\Pi_i)$ and $p(\Pi_i)$, we have

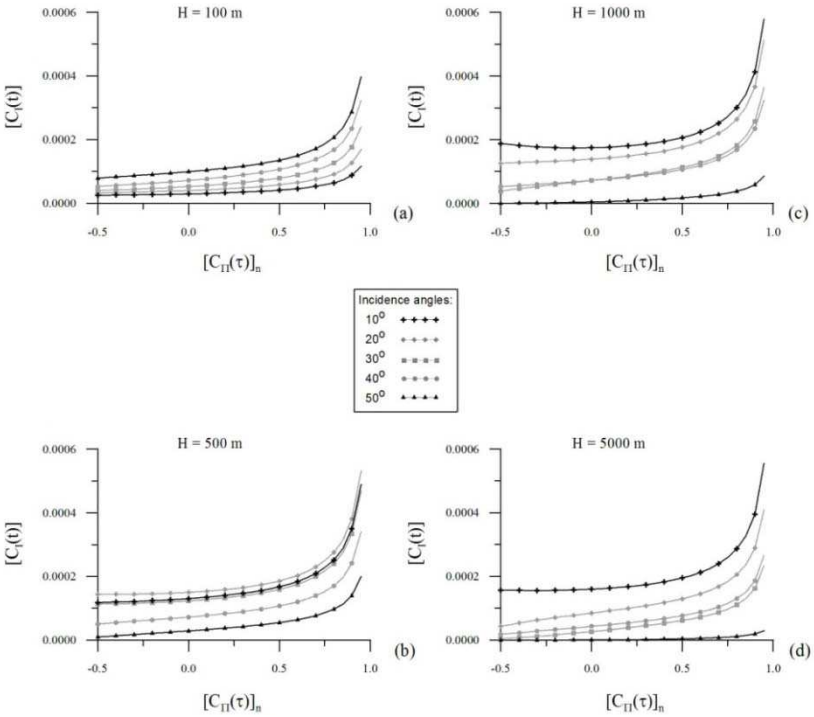

Fig. 7. Relationship between the correlation function of the surface slopes and the correlation function of the intensities in the image.

$$\mu_I = \frac{1}{N}\sum_{i=1}^{N}\frac{1}{\sigma_\Pi\sqrt{2\pi}}\int_{-\infty}^{+\infty} rect\left[\frac{\Pi_i-\Pi_{oi}}{\left(1+\Pi_{oi}^2\right)\frac{\beta}{2}}\right]\exp\left(-\frac{\Pi_i^2}{2\sigma_\Pi^2}\right)\bullet\left[\begin{array}{l}1+\frac{1}{6}\lambda_\Pi^{(3)}\left\{\left(\frac{\Pi_i}{\sigma_\Pi}\right)^3-3\left(\frac{\Pi_i}{\sigma_\Pi}\right)\right\}\\+\frac{1}{24}\lambda_\Pi^{(4)}\left\{\left(\frac{\Pi_i}{\sigma_\Pi}\right)^4-6\left(\frac{\Pi_i}{\sigma_\Pi}\right)^2+3\right\}\end{array}\right]d\Pi_i. \quad (40)$$

The detector angle θ_d is a function of the position x, thus, the specular angle is a function of the distance x from the nadir point of the detector, n = 0, to the point n = i (see equation (22)). Writing again $a_i = \Pi_{oi} - \left(1+\Pi_{oi}^2\right)\beta/4$ and $b_i = \Pi_{oi} + \left(1+\Pi_{oi}^2\right)\beta/4$, we can write

$$\mu_I = \frac{1}{N}\sum_{i=1}^{N}\left\{\begin{array}{l}\left[erf\left(\frac{b_i}{\sqrt{2}\sigma_\Pi}\right)-erf\left(\frac{a_i}{\sqrt{2}\sigma_\Pi}\right)\right]\bullet\left[\frac{1}{2}+\frac{1}{8}\lambda_\Pi^{(4)}\left(1-3\sigma_\Pi^2\right)\right]+\\+\exp\left(-\frac{a_i^2}{2\sigma_\Pi^2}\right)\bullet\left[\frac{\lambda_\Pi^{(3)}}{6\sqrt{2\pi}\sigma_\Pi^2}\left(a_i^2-\sigma_\Pi^2\right)+\frac{\lambda_\Pi^{(4)}a_i}{24\sqrt{2\pi}\sigma_\Pi^3}\left(a_i^2-3\sigma_\Pi^2\right)\right]+\\+\exp\left(-\frac{b_i^2}{2\sigma_\Pi^2}\right)\bullet\left[\frac{\lambda_\Pi^{(3)}}{6\sqrt{2\pi}\sigma_\Pi^2}\left(\sigma_\Pi^2-b_i^2\right)+\frac{\lambda_\Pi^{(4)}b_i}{24\sqrt{2\pi}\sigma_\Pi^3}\left(3\sigma_\Pi^2-b_i^2\right)\right]\end{array}\right\}. \quad (41)$$

The variance of the intensities in the image σ_I^2 is defined by equation (33). Substituting equation (41) in equation (33) we have

$$\sigma_I^2 = \frac{1}{N}\sum_{i=1}^{N}\left\{\begin{array}{l}\left[erf\left(\frac{b_i}{\sqrt{2}\sigma_\Pi}\right)-erf\left(\frac{a_i}{\sqrt{2}\sigma_\Pi}\right)\right]\bullet\left[\frac{1}{2}+\frac{1}{8}\lambda_\Pi^{(4)}\left(1-3\sigma_\Pi^2\right)\right]+\\ +\exp\left(-\frac{a_i^2}{2\sigma_\Pi^2}\right)\bullet\left[\frac{\lambda_\Pi^{(3)}}{6\sqrt{2\pi}\sigma_\Pi^2}\left(a_i^2-\sigma_\Pi^2\right)+\frac{\lambda_\Pi^{(4)}a_i}{24\sqrt{2\pi}\sigma_\Pi^3}\left(a_i^2-3\sigma_\Pi^2\right)\right]+\\ +\exp\left(-\frac{b_i^2}{2\sigma_\Pi^2}\right)\bullet\left[\frac{\lambda_\Pi^{(3)}}{6\sqrt{2\pi}\sigma_\Pi^2}\left(\sigma_\Pi^2-b_i^2\right)+\frac{\lambda_\Pi^{(4)}b_i}{24\sqrt{2\pi}\sigma_\Pi^3}\left(3\sigma_\Pi^2-b_i^2\right)\right]\end{array}\right\}-$$

$$\frac{1}{N^2}\left[\sum_{i=1}^{N}\left\{\begin{array}{l}\left[erf\left(\frac{b_i}{\sqrt{2}\sigma_\Pi}\right)-erf\left(\frac{a_i}{\sqrt{2}\sigma_\Pi}\right)\right]\bullet\left[\frac{1}{2}+\frac{1}{8}\lambda_\Pi^{(4)}\left(1-3\sigma_\Pi^2\right)\right]+\\ +\exp\left(-\frac{a_i^2}{2\sigma_\Pi^2}\right)\bullet\left[\frac{\lambda_\Pi^{(3)}}{6\sqrt{2\pi}\sigma_\Pi^2}\left(a_i^2-\sigma_\Pi^2\right)+\frac{\lambda_\Pi^{(4)}a_i}{24\sqrt{2\pi}\sigma_\Pi^3}\left(a_i^2-3\sigma_\Pi^2\right)\right]+\\ +\exp\left(-\frac{b_i^2}{2\sigma_\Pi^2}\right)\bullet\left[\frac{\lambda_\Pi^{(3)}}{6\sqrt{2\pi}\sigma_\Pi^2}\left(\sigma_\Pi^2-b_i^2\right)+\frac{\lambda_\Pi^{(4)}b_i}{24\sqrt{2\pi}\sigma_\Pi^3}\left(3\sigma_\Pi^2-b_i^2\right)\right]\end{array}\right\}\right]^2 \quad (42)$$

which is the required relationship between the variance of the intensities in the image σ_I^2 and the variance of the surface slopes σ_Π^2 when a non-Gaussian probability density function is considered.

The relationship between the variance of the surface slopes and the variances of the intensities of the image for different θ_s angles (10°-50°) is shown in figures 8 and 9 (equation 42). Figures 8 and 9 show this relationship considering the skewness and the skewness and kurtosis in the non-Gaussian probability density function respectively. We can see that the behavior of the curves looks very similar to the Gaussian case (figure 6). The values for skewness and kurtosis were taken from a Table showed by Plant (2003) from data given by Cox & Munk (1956), for a wind speed of 13.3 m/s with the wind sensor at 12.5 m on the sea surface level.

The curves including the skewness and skewness and kurtosis are little higher for small values of σ_Π^2 compared with the Gaussian case (figure 6) except when θ_s is below 40° where the Gaussian and non-Gaussian cases (considering skewness only) are inverted to small surface slope variances, and these results show that σ_I^2 increases for higher θ_s values (figures 8a and 9a). Cox & Munk (1956) reported σ_Π^2 values of 0.04 and 0.05 like maximum values of the surface slopes in the wind direction and values of 0.03 in the cross wind direction for wind speed bigger than 10 m/s. Thus, we think that in the range for σ_Π^2 from 0-0.05 the behavior of the curves look very clear and separate each one of the other (figures 8a and 9a). If we analyze the figures 8j and 9j we can observe that σ_I^2 increases for lower θ_s values (10°-20°).

Figures 8 and 9 show how these relationships (σ_I^2 versus σ_Π^2) are changing while H is being bigger, where the skewness and skewness and kurtosis are being considered. These curves have the same behavior like in the Gaussian case and the explanation for this inversion is the same as explained before.

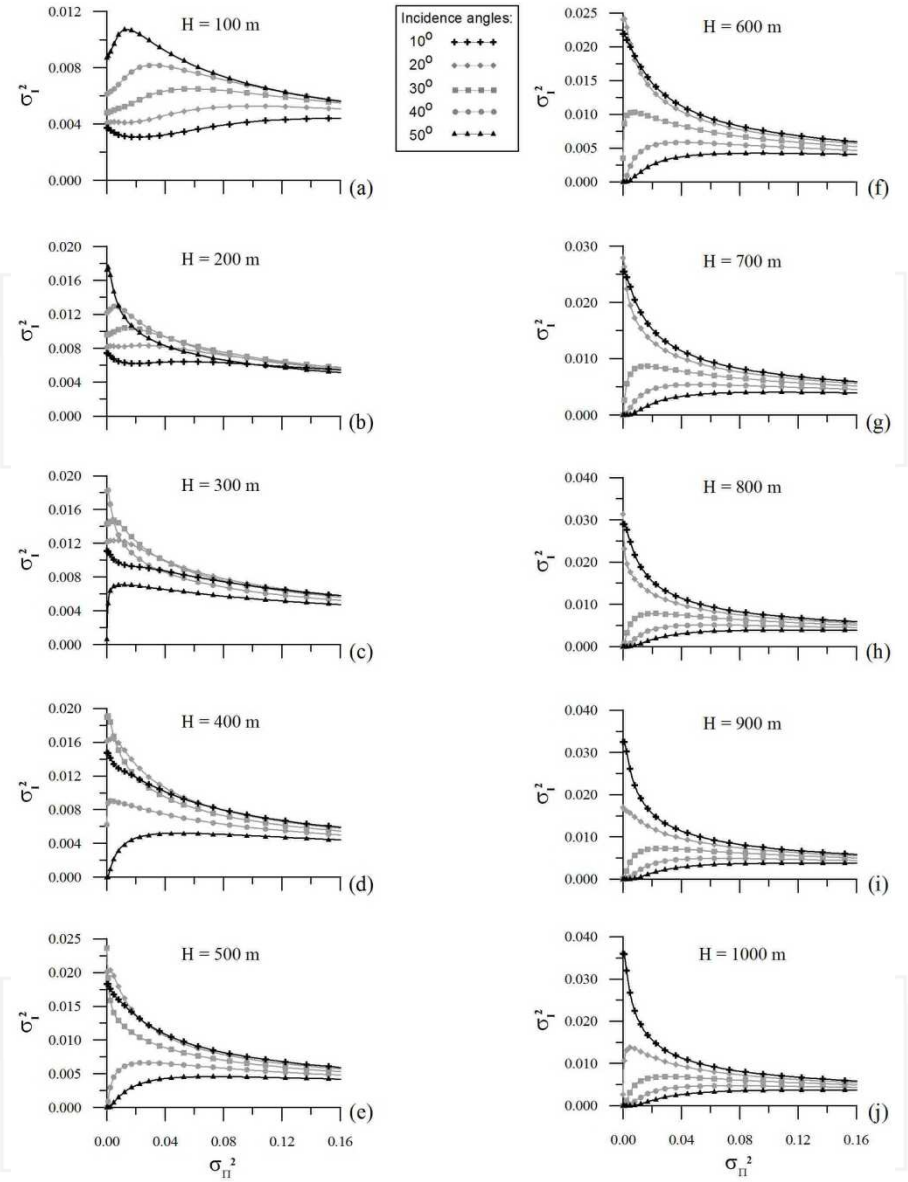

Fig. 8. Relationship between the variance of the surface slopes and the variance of the intensities of the image, for different H values considering a non-Gaussian probability density function where the skewness has been taken account only.

About the non-Gaussian case we can conclude that the main difference with the Gaussian case is the less higher values of the variance of the intensities of the image for small values of surface slope variance when θ_s is in the 40° – 50° range when H=100 m. In addition, when

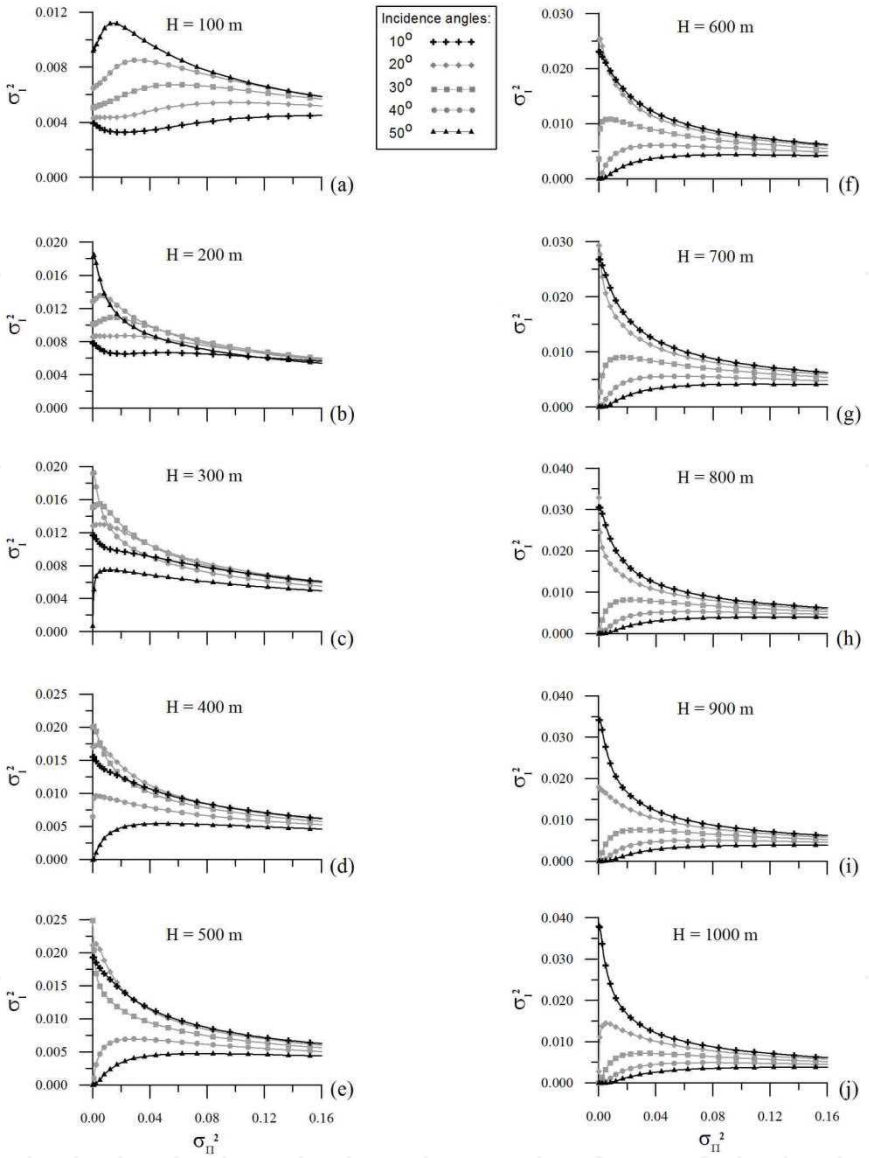

Fig. 9. Relationship between the variance of the surface slopes and the variance of the intensities of the image, for different H values considering a non-Gaussian probability density function where the skewness and kurtosis have been taken account.

H=1000 m this condition is inverted, we can find less smaller values of the variance of the intensities of the image for small values of surface slope variance when θ_s is in the 10° – 20° range. In the other angles, in both cases, it is not possible to see significant differences between the values 10° – 30° when H=100 m and 30° – 50° when H=1000 m.

4.2 Relationship between the correlation functions of the intensities in the image and of the surface slope considering a non-Gaussian probability density function

As mentioned before, our analysis involves three random processes: the surface profile $\zeta(x)$, its surface slopes $\Pi(x)$ and the image $I(x)$. Each process has a correlation function and it was shown in (Álvarez-Borrego, 1993) that these three functions are related.

The relationship between the correlation function of the surface slopes $C_\Pi(\tau)$ and the correlation function of the intensities in the image $C_I(\tau)$ is given by

$$\sigma_I^2 C_I(\tau) = \frac{1}{N}\sum_{i=1}^{N}\int_{-\infty}^{\infty}\frac{1}{N}\sum_{i=1}^{N}\int_{-\infty}^{\infty} B(\Pi_{1i})B(\Pi_{2i})p(\Pi_{1i},\Pi_{2i})\,d\Pi_{1i}\,d\Pi_{2i}, \tag{43}$$

where $p(\Pi_{1i},\Pi_{2i})$ is defined by (Cureton, 2010)

$$p(\Pi_{1i},\Pi_{2i}) = \frac{1}{2\pi\sigma_\Pi^2\left[1-C_\Pi^2(\tau)\right]^{1/2}}\exp\left[-\frac{\Pi_{1i}^2 - 2C_\Pi(\tau)\Pi_{1i}\Pi_{2i} + \Pi_{2i}^2}{2\sigma_\Pi^2\left(1-C_\Pi^2(\tau)\right)}\right]\times$$
$$\left\{1+\frac{1}{6}\left\{\begin{array}{l}\lambda_\Pi^{(30)}\left[\left(\frac{\Pi_{1i}}{\sigma_\Pi}\right)^3 - 3\sigma_\Pi^2\left(\frac{\Pi_{1i}}{\sigma_\Pi}\right)\right]+\\ 3\lambda_\Pi^{(21)}\left[\left(\frac{\Pi_{1i}}{\sigma_\Pi}\right)^2\left(\frac{\Pi_{2i}}{\sigma_\Pi}\right) - \sigma_\Pi^2\left(\frac{\Pi_{2i}}{\sigma_\Pi}\right) + 2\sigma_\Pi^2 C_\Pi(\tau)\left(\frac{\Pi_{1i}}{\sigma_\Pi}\right)\right]+\\ 3\lambda_\Pi^{(12)}\left[\left(\frac{\Pi_{1i}}{\sigma_\Pi}\right)\left(\frac{\Pi_{2i}}{\sigma_\Pi}\right)^2 - \sigma_\Pi^2\left(\frac{\Pi_{1i}}{\sigma_\Pi}\right) + 2\sigma_\Pi^2 C_\Pi(\tau)\left(\frac{\Pi_{2i}}{\sigma_\Pi}\right)\right]+\\ \lambda_\Pi^{(03)}\left[\left(\frac{\Pi_{2i}}{\sigma_\Pi}\right)^3 - 3\sigma_\Pi^2\left(\frac{\Pi_{2i}}{\sigma_\Pi}\right)\right]\end{array}\right\}\right\}, \tag{44}$$

where $\lambda_\Pi^{(03)}$ and $\lambda_\Pi^{(30)}$ are the skewness, $\lambda_\Pi^{(12)}$ and $\lambda_\Pi^{(21)}$ are the relationship between the moments of Π_{1i} and Π_{2i}.

Although it is possible to obtain an analytical relationship for the first integral, for the second integral the process must be numeric. Thus, equation (43) can be written like

$$\sigma_I^2 C_I(\tau) = \frac{1}{N}\sum_{i=1}^{N}\int_{a_i}^{b_i}\frac{1}{N}\sum_{i=1}^{N}\exp\left(-\frac{\Pi_{2i}}{2\sigma_\Pi^2}\right)\times\left\{\begin{array}{l}\exp\left[-(ub_i+v\Pi_{2i})^2\right]\times\left(A_1\Pi_{2i}^2 + B_1 b_i\Pi_{2i} + C_1\right)\\ +\exp\left[-(ua_i+v\Pi_{2i})^2\right]\times\left(A_2\Pi_{2i}^2 + B_2 a_i\Pi_{2i} + C_2\right)\\ +\left[erf(ub_i+v\Pi_{2i}) - erf(ua_i+v\Pi_{2i})\right]\times\left(A_3\Pi_{2i}^3 + B_3\Pi_{2i} + C_3\right)\end{array}\right\}d\Pi_{2i}, \tag{45}$$

where

$$u = \frac{1}{\sqrt{2\sigma_\Pi^2\left[1-C_\Pi^2(\tau)\right]}},$$

$$v = \frac{-C_{\Pi}(\tau)}{\sqrt{2\sigma_{\Pi}^{2}\left[1-C_{\Pi}^{2}(\tau)\right]}},$$

$$A_1 = -\frac{\sqrt{1-C_{\Pi}^{2}(\tau)}}{12\pi\sigma_{\Pi}^{3}}\left(C_{\Pi}^{2}(\tau)\lambda_{\Pi}^{(30)} + 3C_{\Pi}(\tau)\lambda_{\Pi}^{(21)} + 3\lambda_{\Pi}^{(12)}\right) = -A_2,$$

$$B_1 = -\frac{\sqrt{1-C_{\Pi}^{2}(\tau)}}{12\pi\sigma_{\Pi}^{3}}\left(C_{\Pi}(\tau)\lambda_{\Pi}^{(30)} + 3\lambda_{\Pi}^{(21)}\right) = -B_2,$$

$$C_1 = -\frac{\sqrt{1-C_{\Pi}^{2}(\tau)}}{12\pi\sigma_{\Pi}^{3}}\left[\left(b_i^2 + 2\sigma_{\Pi}^{2}\left[1-C_{\Pi}^{2}(\tau)\right] - 3\sigma_{\Pi}^{4}\right)\lambda_{\Pi}^{(30)} + 6\sigma_{\Pi}^{4}C_{\Pi}(\tau)\lambda_{\Pi}^{(21)} - 3\sigma_{\Pi}^{4}\lambda_{\Pi}^{(12)}\right],$$

$$C_2 = \frac{\sqrt{1-C_{\Pi}^{2}(\tau)}}{12\pi\sigma_{\Pi}^{3}}\left[\left(a_i^2 + 2\sigma_{\Pi}^{2}\left[1-C_{\Pi}^{2}(\tau)\right] - 3\sigma_{\Pi}^{4}\right)\lambda_{\Pi}^{(30)} + 6\sigma_{\Pi}^{4}C_{\Pi}(\tau)\lambda_{\Pi}^{(21)} - 3\sigma_{\Pi}^{4}\lambda_{\Pi}^{(12)}\right],$$

$$A_3 = \frac{\sqrt{2}}{24\sqrt{\pi}\sigma_{\Pi}^{4}}\left(C_{\Pi}^{3}(\tau)\lambda_{\Pi}^{(30)} + 3C_{\Pi}^{2}(\tau)\lambda_{\Pi}^{(21)} + 3C_{\Pi}(\tau)\lambda_{\Pi}^{(12)} + \lambda_{\Pi}^{(03)}\right),$$

$$B_3 = \frac{\sqrt{2}}{8\sqrt{\pi}}\left[C_{\Pi}(\tau)\left(\frac{1-C_{\Pi}^{2}(\tau)}{\sigma_{\Pi}^{2}} - 1\right)\lambda_{\Pi}^{(30)} + \left(2C_{\Pi}^{2}(\tau) + \frac{1-C_{\Pi}^{2}(\tau)}{\sigma_{\Pi}^{2}} - 1\right)\lambda_{\Pi}^{(21)} + C_{\Pi}(\tau)\lambda_{\Pi}^{(12)} - \lambda_{\Pi}^{(03)}\right],$$

$$C_3 = \frac{\sqrt{2}}{4\sqrt{\pi}\sigma_{\Pi}}.$$

Figure 10 shows graphically the relationship between the normalized correlation function of the surface slopes $\left[C_{\Pi}(\tau)\right]_n$ and the normalized correlation function of the intensities of the image $\left[C_I(\tau)\right]_n$. In this case a $\sigma_{\Pi}^2 = 0.03$ was used. When H increases the behavior of the curves have a similar process like the variance curves.

When H=100 m (Figure 10a) the behavior of the curves for θ_s of 10º – 20º have an "unusual" behavior for low surface slope variances when compared with Gaussian case. This is because the inversion of the curves starts to lower values of H. In order to avoid memory computer problems, the 16384 data points profile was divided into a number of consecutive intervals. The value of θ_d varies point to point in the profile. For each interval and for each θ_s value, the relationship between the correlation functions $C_I(\tau)$ and $C_{\Pi}(\tau)$ was calculated. Then, all the computed relationships for each θ_s value were averaged.

A theoretical variance σ_I^2 can be calculated from equation (45). We wrote in Table 3 the values of the image variance in order to normalize the correlations in figure 10 for different values for θ_s and H (100, 500, 1000 and 5000 m).

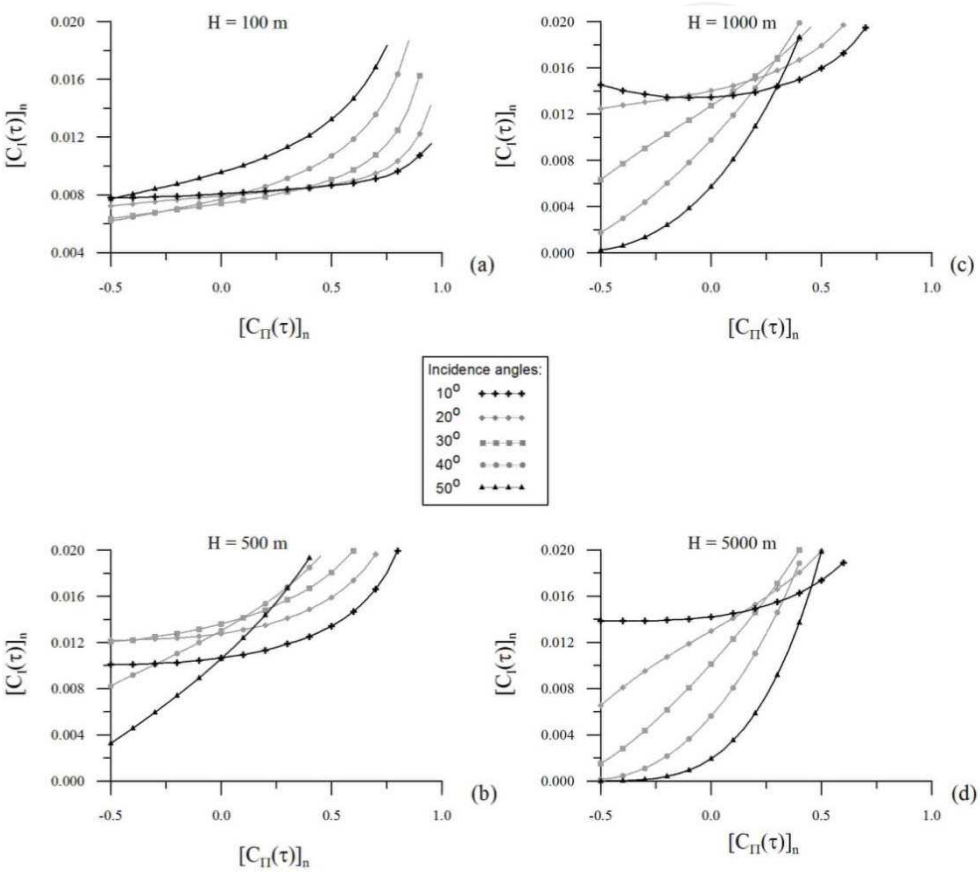

Fig. 10. Relationship between the correlation function of the surface slopes and the correlation function of the intensities in the image. The curves correspond to different values of θ_s .

H	θ_s	σ_Π^2	σ_I^2
100	10	0.03	0.003126364
100	20	0.03	0.004354971
100	30	0.03	0.006071378
100	40	0.03	0.008187813
100	50	0.03	0.009875824
500	10	0.03	0.012038690
500	20	0.03	0.011886750
500	30	0.03	0.009668245
500	40	0.03	0.006645083
500	50	0.03	0.003959459
1000	10	0.03	0.012945720
1000	20	0.03	0.010339930
1000	30	0.03	0.006902623
1000	40	0.03	0.004036960
1000	50	0.03	0.002067475
5000	10	0.03	0.011358240
5000	20	0.03	0.007713670
5000	30	0.03	0.004572885
5000	40	0.03	0.002406005
5000	50	0.03	0.001022463

Table 3. Values of the image variance in order to normalize the correlations in figure 10 for different values for θ_s and H.

5. Conclusions

We derive the variance of the surface heights from the variance of the intensities in the image via remote sensing considering a glitter function given by equation (12) when the geometry consider a detector angle of $\theta_d = 0^o$, and considering a glitter function given by the equation (24) considering a geometrically improved model with variable detector line of sight angle, given by figure 4. In this last case, we consider Gaussian statistics and non-Gaussian statistics. We derive the variance of the surface slopes from the variance of the intensities of remote sensed images for different H values. In addition, we discussed the determination of the correlation function of the surface slopes from the correlation function of the image intensities considering Gaussian and non-Gaussian statistics.

Analyzing the variances curves for Gaussian and non-Gaussian case it is possible to see the behavior of the curves for different incident angles when H increases. This behavior agrees with the results presented by Álvarez-Borrego (1993) and Geoff Cureton *et al*. 2007, and Álvarez-Borrego and Martin-Atienza (2010) for the Gaussian case.

These new results solve the inverse problem when it is necessary to analyze the statistical of a real sea surface via remote sensing using the image of the glitter pattern of the marine surface.

6. Acknowledgments

This work was partially supported by CONACyT with grant No. 102007 and SEP-PROMET/103.5/10/5021 (UABC-PTC-225).

7. References

Álvarez-Borrego, J. (1987). Optical analysis of two simulated images of the sea surface. *Proceedings SPIE International Society of the Optical Engineering,* Vol.804, pp.192-200, ISSN 0277-786X

Álvarez-Borrego, J. (1993). Wave height spectrum from sun glint patterns: an inverse problem. *Journal of Geophysical Research,* Vol.98, No.C6, pp. 10245-10258, ISSN 0148-0227

Álvarez-Borrego, J. (1995). Some statistical properties of surface heights via remote sensing. *Journal of Modern Optics,* Vol.42, No.2, pp. 279-288, ISSN 0950-0340

Álvarez-Borrego, J. & Machado M. A. (1985). Optical analysis of a simulated image of the sea surface. *Applied Optics,* Vol.24, No.7, pp. 1064-1072, ISSN 1559-128X

Álvarez-Borrego, J. & Martin-Atienza, B. (2010). An improved model to obtain some statistical properties of surface slopes via remote sensing using variable reflection angle. *IEEE Transactions on Geoscience and Remote Sensing,* Vol.48, No.10, pp. 3647-3651, ISSN 0196-2892

Bréon, F. M. & Henrist N. (2006). Spaceborn observations of ocean glint reflectance and modeling of wave slope distributions. *Journal Geophysical Research,* Vol.111, CO6005, ISSN 0148-0227

Chapman, R. D. & Irani G. B. (1981). Errors in estimating slope spectra from wave images. *Applied Optics,* Vol.20, No.20, pp. 3645-3652, ISSN 1559-128X

Chapron, B.; Vandemark D. & Elfouhaily T. (2002). On the skewness of the sea slope probability distribution. *Gas Transfer at Water Surfaces,* Vol.127, pp. 59-63, ISSN 0875909868

Cox, C. & Munk W. (1954a). Statistics of the sea surface derived from sun glitter. *Journal Marine Research,* Vol.13, No.2, pp. 198-227, ISSN 0022-2402

Cox, C. & Munk W. (1954b). Measurements of the roughness of the sea surface from photographs of the Sun's glitter. *Journal of the Optical Society of America,* Vol.24, No.11, pp. 838-850, ISSN 1084-7529

Cox, C. & Munk W. (1955). Some problems in optical oceanography. *Journal of Marine Research,* Vo.14, pp. 63-78, ISSN 0022-2402

Cox, C. & Munk. W. (1956). Slopes of the sea surface deduced from photographs of sun glitter. *Bulletin of the Scripps Institution of Oceanography,* Vol.6, No.9, pp. 401-488

Cureton, G. P. (2010). *Retrieval of nonlinear spectral information from ocean sunglint*. PhD thesis, Curtin University of Technology, Australia, March

Cureton, G. P.; Anderson, S. J.; Lynch, M. J. & McGann, B. T. (2007). Retrieval of wind wave elevation spectra from sunglint data. *IEEE Transactions on Geoscience and Remote Sensing,* Vol.45, No.9, pp. 2829-2836, ISSN 0196-2892

Fuks, I. M. & Charnotskii, M. I. (2006). Statistics of specular points at a randomly rough surface. *Journal of the Optical Society of America, Optical Image Science,* Vol.23, No.1, pp. 73-80, ISSN 1084-7529

Gaskill, J. D. (1978). *Linear systems, Fourier transform, and optics.* John Wiley & Sons. ISBN 0-471-29288-5, New York, USA

Longuet-Higgins, M. S. (1962). The statistical geometry of random surfaces. *Proceedings Symposium Applied Mathematics 1960 13th Hydrodynamic Instability,* pp. 105-143

Longuet-Higgins, M. S.; Cartwright, D. E. & Smith, N. D. (1963). Observations of the directional spectrum of sea waves using the motions of a floating buoy, In: *Ocean Wave Spectra,* Prentice-Hall, Englewood Cliffs, N. J. (Ed.), 111-136

Munk, W. (2009). An inconvenient sea truth: spread, steepness, and skewness of surface slopes. *Annual Review of Marine Sciences,* Vol.1, pp. 377-415, ISSN 1941-1405

Papoulis, A. (1981). *Probability, Random Variables, and Stochastic Processes,* chapter 9, McGraw-Hill, ISBN 0-07-119981-0, New York, USA

Peppers, N. & Ostrem, J. S. (1978). Determination of wave slopes from photographs of the ocean surface: A new approach. *Applied Optics,* Vol.17, No.21, pp. 3450-3458, ISSN 1559-128X

Plant, W. J. (2003). A new interpretation of sea-surface slope probability density functions. *Journal of Geophysical Research,* Vol.108, No.C9, 3295, ISSN 0148-0227

Stilwell, D. Jr. (1969). Directional energy spectra of the sea from photographs. *Journal of Geophysical Research,* Vol.74, No.8, pp. 1974-1986, ISSN 0148-0227

Stilwell, D. Jr. & Pilon, R. O. (1974). Directional spectra of surface waves from photographs. *Journal of Geophysical Research,* Vol.79, No.9, pp.1277-1284, ISSN 0148-0227

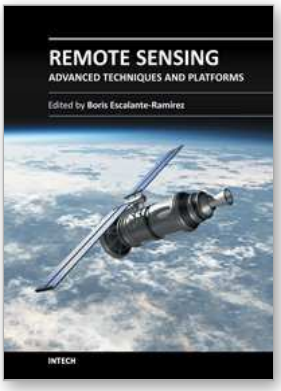

Remote Sensing - Advanced Techniques and Platforms

Edited by Dr. Boris Escalante

ISBN 978-953-51-0652-4

Hard cover, 462 pages

Publisher InTech

Published online 13, June, 2012

Published in print edition June, 2012

This dual conception of remote sensing brought us to the idea of preparing two different books; in addition to the first book which displays recent advances in remote sensing applications, this book is devoted to new techniques for data processing, sensors and platforms. We do not intend this book to cover all aspects of remote sensing techniques and platforms, since it would be an impossible task for a single volume. Instead, we have collected a number of high-quality, original and representative contributions in those areas.

How to reference

In order to correctly reference this scholarly work, feel free to copy and paste the following:

Josué Álvarez-Borrego and Beatriz Martín-Atienza (2012). Statistical Properties of Surface Slopes via Remote Sensing, Remote Sensing - Advanced Techniques and Platforms, Dr. Boris Escalante (Ed.), ISBN: 978-953-51-0652-4, InTech, Available from: http://www.intechopen.com/books/remote-sensing-advanced-techniques-and-platforms/statistical-properties-of-surface-slopes-via-remote-sensing

INTECH
open science | open minds

InTech Europe
University Campus STeP Ri
Slavka Krautzeka 83/A
51000 Rijeka, Croatia
Phone: +385 (51) 770 447
Fax: +385 (51) 686 166
www.intechopen.com

InTech China
Unit 405, Office Block, Hotel Equatorial Shanghai
No.65, Yan An Road (West), Shanghai, 200040, China
中国上海市延安西路65号上海国际贵都大饭店办公楼405单元
Phone: +86-21-62489820
Fax: +86-21-62489821